

LOCUSS: THE MASS DENSITY PROFILE OF MASSIVE GALAXY CLUSTERS AT Z=0.2

NOBUHIRO OKABE¹, GRAHAM P. SMITH², KEIICHI UMETSU¹, MASAHIRO TAKADA³, TOSHIFUMI FUTAMASE⁴*Draft version February 13, 2013*

ABSTRACT

We present a stacked weak-lensing analysis of a complete and volume-limited sample of 50 massive galaxy clusters at $0.15 < z < 0.3$, based on deep, wide-field, high-resolution observations with Suprime-Cam on the 8.2-m Subaru Telescope. Our new approach to selecting lensed background galaxies measures explicitly contamination by unlensed faint cluster and foreground galaxies, enabling us to define a secure sample of background galaxies lying red-ward of the cluster red sequence. We achieve a contamination fraction of just 1% in our background sample, from which we detect the tangential shear signal in the stacked data at a total signal-to-noise ratio of $S/N = 32.7$. The mass distribution reconstructed from the stacked data is nearly circularly-symmetric, and the tangential shear profile is remarkably smooth, justifying a one-dimensional radial analysis of the cluster mass distribution. The universal Navarro-Frenk-White model gives an excellent fit to the data, returning tight constraints on mass, $M_{\text{vir}} = 7.19^{+0.53}_{-0.50} \times 10^{14} h^{-1} M_{\odot}$, and concentration, $c_{\text{vir}} = 5.41^{+0.49}_{-0.45}$ ($c_{200} = 4.22^{+0.40}_{-0.36}$). Our new results confirm and strengthen our previous claim that massive galaxy clusters have shallow density profiles that are broadly in line with predictions from numerical simulations. The sub-10% statistical precision of our measurements is comparable with the differences between the predictions from numerical simulations in the literature.

Subject headings: galaxies: clusters: general — gravitational lensing: weak — cosmology: observations

1. INTRODUCTION

In the cold dark matter structure formation paradigm galaxy clusters are the most massive, and most recently formed collapsed structures. A clear prediction derived from numerical simulations is that the density profile of galaxy clusters should therefore be less concentrated than that of less massive objects – galaxy groups, and individual galaxies (e.g. Bullock et al. 2001; Dolag et al. 2004; Neto et al. 2007; Duffy et al. 2008; Zhao et al. 2009).

Gravitational lensing is a powerful probe of cosmic matter density because the lensing signal is insensitive to the physical nature and state of matter. The density profile of strong-lensing clusters is claimed to be more concentrated than predicted (Gavazzi et al. 2003; Kneib et al. 2003; Broadhurst et al. 2008; Oguri et al. 2009), even after correcting selection biases (Hennawi et al. 2007). Interpretation of these results is complicated by the small size of the observed samples, and the selection of the most spectacular strong-lensing clusters. On the theoretical side, the interpretation is complicated by the intrinsic scatter in profile shapes, and the rarity of massive cluster-scale dark matter halos within the simulated volumes.

Our weak-lensing study of a representative sample of 30 X-ray selected clusters showed that their density profiles agree better with predictions than those of spec-

tacular strong-lensing clusters (Okabe et al. 2010, hereafter Ok10). Oguri et al. (2012) have also shown that less extreme strong-lensing clusters are in better agreement with predictions. Both studies employed stacking techniques to derive the mean properties of clusters, thus reducing the intrinsic shape noise of weak-lensing measurements, and eliminating biases due to the orientation and internal structure of clusters and the projection effect of large-scale structures (see also Johnston et al. 2007).

In this paper, we stack a complete, volume-limited sample of 50 galaxy clusters that we have observed with the Subaru Telescope as part of the Local Cluster Substructure Survey (LoCuSS⁵). The superb image quality, large field of view, and large collecting area of Subaru/Suprime-Cam (Miyazaki et al. 2002) are ideally suited to accurate measurements of faint galaxy shapes that are required for robust weak-lensing analysis (e.g. Ok10). Our sample comprises all clusters from the *ROSAT* All Sky Survey catalogs (Ebeling et al. 1998, 2000; Böhringer et al. 2004) that satisfy $L_X[0.1 - 2.4 \text{ keV}]/E(z)^{2.7} \geq 4.2 \times 10^{44} \text{ erg s}^{-1}$, $0.15 \leq z \leq 0.30$, $n_H < 7 \times 10^{20} \text{ cm}^{-2}$, and $-25^\circ < \delta < +65^\circ$. where $E(z) \equiv H(z)/H_0$ is the normalized Hubble expansion rate, and selecting on $L_X/E(z)^{2.7}$ mimics a mass selection (Popesso et al. 2005).

In §2 we describe our data and analysis; in §3 we explain our results and compare with numerical simulations; in §4 we summarize our conclusions. We use the concordance Λ CDM model of $\Omega_{M,0} = 0.27$, $\Omega_{\Lambda} = 0.73$ and $H_0 = 100h \text{ km s}^{-1} \text{ Mpc}^{-1}$ (Komatsu et al. 2011). In this cosmology the virial over-density at the mean redshift of our cluster sample, $\langle z \rangle = 0.23$ is $\Delta_{\text{vir}} = 113.77$. All error bars are 68% confidence intervals unless otherwise stated.

¹ Academia Sinica Institute of Astronomy and Astrophysics (ASIAA), P. O. Box 23-141, Taipei 10617, Taiwan; okabe@asiaa.sinica.edu.tw

² School of Physics and Astronomy, University of Birmingham, Edgbaston, Birmingham, B15 2TT, England; gps@star.sr.bham.ac.uk

³ Kavli Institute for the Physics and Mathematics of the Universe (Kavli IPMU, WPI), The University of Tokyo, Chiba 277-8582, Japan

⁴ Astronomical Institute, Tohoku University, Aramaki, Aoba-ku, Sendai, 980-8578, Japan

⁵ <http://www.sr.bham.ac.uk/locuss>

2. SUBARU DATA AND WEAK-LENSING ANALYSES

Sensitive wide-field optical imaging of all 50 clusters is available from the Subaru/Suprime-Cam⁶⁷. The observations, data reduction, and analysis will be described in detail in a future article. In brief, all 50 clusters were observed through two filters, 46 through V/i' -band filters, 2 each through the V/I_C - and g/i' -band filters. Hereafter we refer to the bluer filter as V and the redder filter as i' . All data were reduced using standard routines (Ok10). The full-width half maximum of point sources in the reduced V/i' -band frames is $0''.6 \lesssim \text{FWHM} \lesssim 0''.9$ and $0''.5 \lesssim \text{FWHM} \lesssim 0''.7$, respectively. Photometric calibration to $\leq 10\%$ precision in both filters was achieved via observations of Landolt standard stars, and double checked against SDSS/DR8 stellar photometry (Eisenstein et al. 2011). We corrected for galactic extinction (Schlafly & Finkbeiner 2011).

We measure the shape of faint galaxies using a modified version of Ok10's pipeline, which is based on the IMCAT⁸ implementation of the Kaiser et al. (1995, hereafter, KSB) method. The main modification is that we calibrate the KSB isotropic correction factor for individual objects using a subset of galaxies detected with high significance $\nu > 30$ (Umetsu et al. 2010). This minimizes the shear calibration bias that is inherent to KSB+ methods in the presence of measurement errors (Okura & Futamase 2012).

We confirmed the reliability of our shape measurements using simulated data that were generated using GLAFIC (Oguri 2010) with point spread functions described by the Moffat profile with a range of seeing ($0''.5 < \text{FWHM} < 1''.1$) and power indices ($3 < \beta < 12$), as described in Oguri et al. (2012). We obtain a multiplicative calibration bias (m) and additive residual shear offset (c) (see Heymans et al. 2006; Massey et al. 2007, for definitions) of $|m| \lesssim 0.03$ and $|c| \lesssim 2 \times 10^{-4}$, respectively, for $\text{FWHM} \simeq 0''.7$.

We define a secure sample of background galaxies based on their color offset from the red sequence of early-type galaxies in the $(V - i')/i'$ color-magnitude plane for each cluster. In the absence of dust-reddening, intrinsic scatter in galaxy colors, and measurement errors, selecting galaxies redder than the red sequence (hereafter “red galaxies”; $\Delta C \equiv (V - i') - (V - i')_{\text{ES0}} > 0$) yields solely background galaxies. However, in reality a non-zero color cut is required to eliminate contamination by faint red cluster galaxies. In contrast, interpretation of “blue galaxy” ($\Delta C < 0$) samples is complicated by star-formation. We discuss red and blue galaxies below,

⁶ Based in part on observations obtained at the Subaru Observatory under the Time Exchange program operated between the Gemini Observatory and the Subaru Observatory. The Gemini Observatory is operated by the Association of Universities for Research in Astronomy, Inc., under a cooperative agreement with the NSF on behalf of the Gemini partnership: the National Science Foundation (United States), the Science and Technology Facilities Council (United Kingdom), the National Research Council (Canada), CONICYT (Chile), the Australian Research Council (Australia), Ministério da Ciência, Tecnologia e Inovação (Brazil) and Ministerio de Ciencia, Tecnología e Innovación Productiva (Argentina).

⁷ Based in part on data collected at Subaru Telescope and obtained from the SMOKA, which is operated by the Astronomy Data Center, National Astronomical Observatory of Japan.

⁸ <http://www.ifa.hawaii/kaiser/IMCAT>

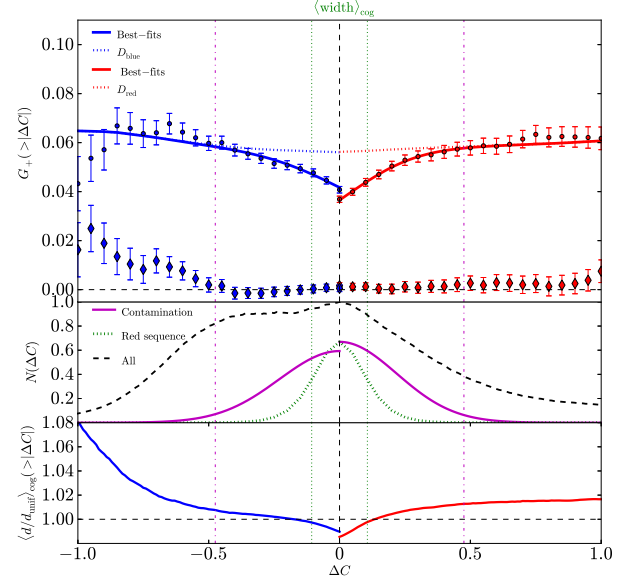


FIG. 1.— TOP: Stacked reduced shear G_+ , as defined in §2, as a function of color offset from the stacked cluster red sequence (filled circles). Filled diamonds show the mean shear calculated after rotating all galaxies through 45° . Solid curves show the best-fit lensing kernel plus contamination model of the trend of G_+ with ΔC . The vertical dashed-dotted magenta line shows the color cut at which the fraction of contaminants is 1%. MIDDLE: The color distribution of all galaxies at $21 < i' < 26$ (black dashed curve). The width of the red sequence of bright ($i' < 20$) cluster members is shown as the green dotted curve, with the green vertical lines de-marking the 1σ width of the red sequence. The magenta curves show the color distribution of contaminants in our model, and upon which the 1% contamination cut is based. BOTTOM: The mean distance with respect to the brightest cluster galaxy for 50 clusters, normalized by a uniform distribution.

retaining only red galaxies for our main analysis and results.

The mean tangential distortion strength averaged over (i) all galaxies satisfying each color cut, (ii) cluster-centric radii of $0.1 h^{-1}\text{Mpc} < r < 2.8 h^{-1}\text{Mpc}$, and (iii) all 50 clusters, $G_+ \equiv \langle \langle g_+ \rangle \rangle$, increases monotonically with ΔC for red galaxies (Fig. 1, upper panel). We interpret the steep slope at $\Delta C \lesssim 0.3$ as arising from contamination by faint red cluster members. Indeed, the mean cluster-centric radius of red galaxies is an increasing function of ΔC at small ΔC , supporting this interpretation (Fig. 1, lower panel). At $\Delta C \gtrsim 0.4$ we interpret the shallow slope of G_+ as arising from a slowly increasing redshift of the faint red background population as ΔC grows.

We therefore fit a two component model to the data. One component describes the color distribution of the contaminating population as a Gaussian centered at $\Delta C = 0$, with standard deviation σ . The other component describes the expected dependence of G_+ on ΔC in the absence of contamination, and is based on the mean lensing kernel, $D(\Delta C) \equiv \langle D_{ls}/D_s \rangle$, for galaxies in the COSMOS photometric redshift catalog (Ilbert et al. 2009) that matches each color cut. The model for the color-dependence of G_+ is therefore: $G_+(\Delta C) = A D(\Delta C) (1 - B f(\Delta C))$, where A is a normalization factor (required to convert D into shear in a simple manner),

B is the normalization of the Gaussian contaminant function at $\Delta C = 0$, and $f(\Delta C > 0) = [1 - \text{erf}(\Delta C/\sqrt{2}\sigma)]/2$. This model has three free parameters: A , B , and σ .

The best-fit model describes the data well (Fig. 1, upper panel). Interestingly, the best-fit standard deviation of the Gaussian is $\sigma = 0.21$. This is larger than expected based on the width of the cluster red sequence for bright galaxies and the photometric errors on faint galaxies, suggesting intrinsic scatter in the color of faint red cluster galaxies. The model describes explicitly the dependence of contaminating fraction on ΔC . We conservatively adopt a limit of 1% on contaminating fraction, which translates into a color cut of $\Delta C > 0.475$. We select galaxies redder than this cut for the results presented in §3; the mean number density of these galaxies is $5.3 \pm 1.0 \text{ arcmin}^{-2}$ per cluster, where the uncertainty is the standard deviation among the 50 clusters. We therefore achieve a total stacked number density of $266.3 \text{ arcmin}^{-2}$.

We applied the same methods to blue galaxies, describing the contaminating fraction as $f(\Delta C < 0) = [1 + \text{erf}(\Delta C/\sqrt{2}\sigma)]/2$. The model does not describe the blue galaxies well, likely due to the non-monotonic color-redshift relationship for these galaxies. We also note that the faint blue population appear to be preferentially found at large cluster centric radii (Fig. 1, lower panel), suggesting that blue galaxy contamination may be dominated by galaxies in the cluster outskirts.

3. RESULTS

We detect each of the 50 clusters at a typical peak signal-to-noise ratio of $S/N \simeq 4$ in two-dimensional Kaiser & Squires (1993) mass reconstructions. We also stack the shear catalogs in physical length units centered on the respective BCGs and reconstruct the average mass distribution of the clusters. The mass density contours become progressively rounder and the significance of the weak-lensing detection increases as more clusters are stacked. The averaged mass map for the full sample is remarkably symmetrical, with a pronounced mass peak of $S/N \simeq 27.5$ (Fig. 2).

Similarly, the stacked tangential shear profile achieves a high statistical precision (Fig. 3). Our stacking procedure follows Umetsu et al. (2011). In brief, we stack in physical length units, centering the catalogs on the respective BCGs, and stack across the radial range $100 h^{-1} \text{ kpc} < r < 2.8 h^{-1} \text{ Mpc}$ in 14 log-spaced bins. We detect the signal at $S/N = 32.7$ using the full covariance matrix to take into account projected uncorrelated large-scale structure and intrinsic ellipticity noise (e.g. Hoekstra 2003; Hoekstra et al. 2011; Oguri & Takada 2011; Umetsu et al. 2011; Oguri et al. 2012), computing the cosmic-shear contribution using the non-linear matter power spectrum (Smith et al. 2003) for the WMAP7 cosmology and the shape noise from the diagonal matrix. The 45°-rotated distortion component is consistent with a null signal, confirming that residual systematic errors are at least an order of magnitude smaller than the measured lensing signal.

The observed density profile of massive galaxy clusters at $z = 0.23$ is clearly curved (Fig 3), and is well-described by the parametric form proposed by Navarro et al. (1997, so-called NFW profile): $\rho \propto x^{-1}(1+x)^{-2}$, where $x \equiv$

r/r_s , and r_s is the radius at which $d \log \rho / d \log r = -2$. We express our model fits in terms of the virial mass $M_{\text{vir}} \equiv (4\pi/3)\rho_{\text{cr}} \Delta_{\text{vir}} r_{\text{vir}}^3$, and the concentration parameter $c_{\text{vir}} \equiv r_{\text{vir}}/r_s$, where Δ_{vir} is the virial over-density and ρ_{cr} is the critical density. We measure both parameters to sub-10% precision (Table 1), obtaining a best fit concentration parameter of $c_{\text{vir}} = 5.4 \pm 0.5$. This result changes by just $\Delta c_{\text{vir}} \simeq 0.1$ when we vary the number of bins between 8 and 18, change the inner radial cut from 80 to 200 $h^{-1} \text{ kpc}$ or the outer radial cut between 2.5 and 3.5 $h^{-1} \text{ Mpc}$. The stability of our results under variations of the inner radial cut underlines the robustness of our new approach to selecting red galaxies, and the negligible level of $\langle \Sigma_{\times} \rangle$ noted above. Finally, we note that our constraints on concentration are stable to $\Delta c_{\text{vir}} \lesssim 0.2$ with respect to increasing the color cut beyond $\Delta C > 0.475$, and to fitting only to galaxies brighter than $i' = 25$. The constraints on M_{vir} are stable to a few per cent under the same tests.

We also investigate whether our stacking procedure introduces systematic errors. We use analytic NFW halos, that match the mass-concentration relation predicted from numerical simulations, to create synthetic weak shear catalogs. These synthetic catalogs match the number density and the field of view of our Subaru data. We draw 300 samples of 50 clusters from the predicted cluster distribution, and stack the respective shear profiles in both physical length units and length units scaled to r_{200} of each analytic NFW halo. We do not detect any bias in the measured mean concentration of the stacked clusters, obtaining $\langle c/c_{\text{truth}} \rangle = 1.02 \pm 0.07$, and $\langle c/c_{\text{truth}} \rangle = 1.08 \pm 0.07$ for stacking in physical length units and re-scaled length units respectively. In both cases we obtain $\langle M/M_{\text{truth}} \rangle = 0.96 \pm 0.06$, and the quoted uncertainties are the standard deviation on 300 samples. The non-detection of a systematic error arising from stacking in physical units is consistent with Ok10's result that their mass-concentration relations from individual and stacked clusters (using physical length units) are self-consistent. We also note that stacking in rescaled length units weights the contribution of each cluster to each bin in a nonlinear and model-dependent manner: $w \propto \theta \Delta \theta \propto r_{200}^2 \propto M_{200}^{2/3}$. The impact of this weighting scheme deserves further detailed investigation in future studies.

The test described above is idealized in that real clusters are aspherical, are embedded in the large-scale-structure, and contain baryons. Tests based on numerically simulated clusters should allow these issues to be investigated in detail in a future article. Here we conduct a preliminary test using clusters extracted from the new ‘‘Cosmo-OWLS’’ simulation that implements the AGN model described in McCarthy et al. (2011) in a 400 $h^{-1} \text{ Mpc}$ box, the weak-lensing catalogs were constructed following Bahé et al. (2012). The results are consistent with the analytic NFW tests described above – the systematic error on the measurement of concentration based on stacking in physical length units is subdominant to the statistical errors, and the central value on the estimated systematic error on stacking in rescaled length units is a factor of several larger than that on stacking in physical length units.

Our statistical errors on concentration are com-

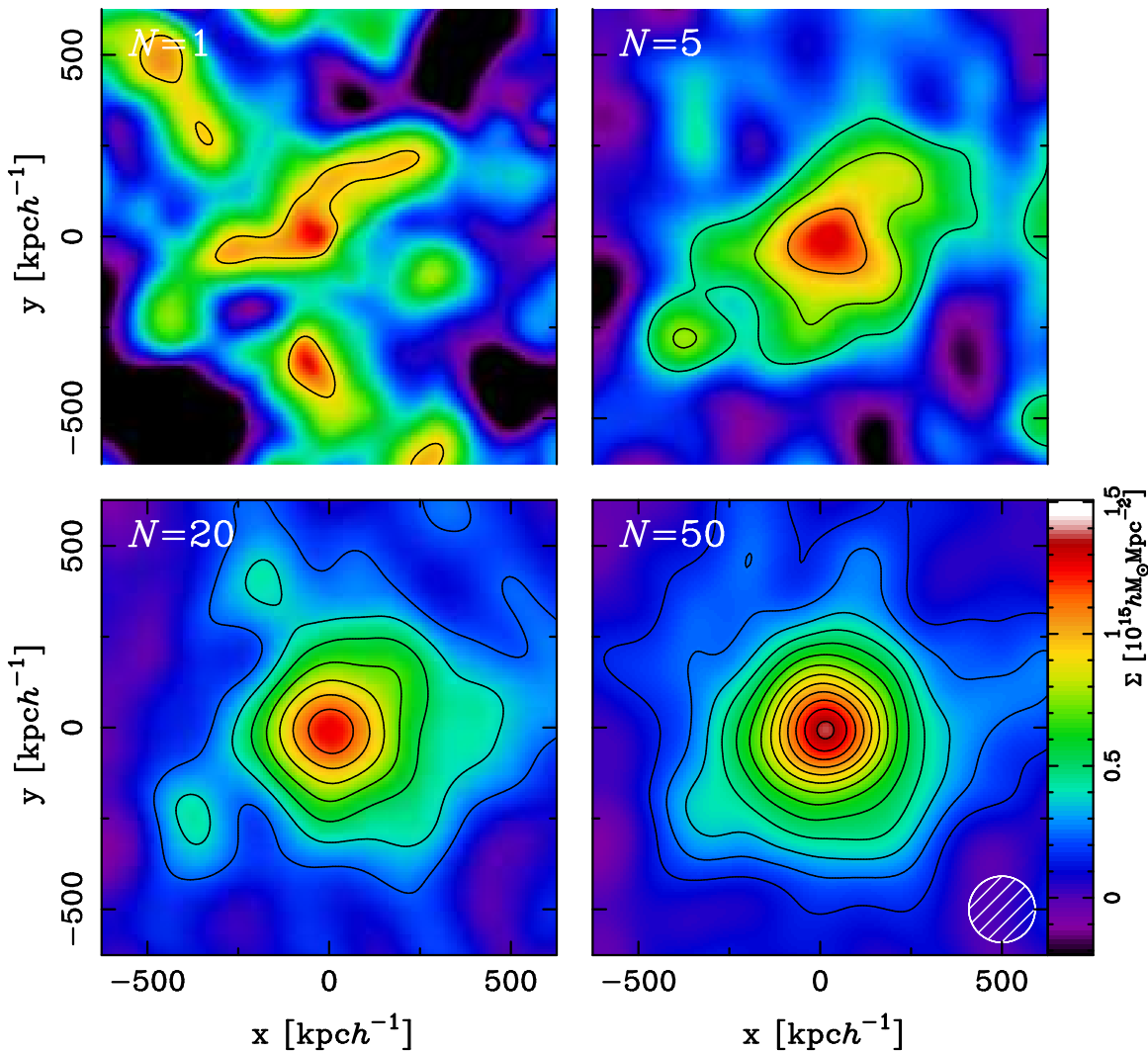


FIG. 2.— The projected mass distribution reconstructed from our weak-lensing catalogs: one typical cluster (ABELL 0141; upper-left panel), 5 clusters (upper-right), 20 clusters (lower-left) and all 50 clusters (lower-right). Each panel spans $1.2 \times 1.2 h^{-2} \text{Mpc}^2$, with contours starting at $S/N = 3$, and spaced at $\Delta S/N = 2$. A Gaussian smoothing scale of FWHM = 2 arcmin is used in all panels (hatched region at lower right).

TABLE 1
DENSITY PROFILE MODELS

Model	Shape parameter ^a	M_{vir} ($10^{14} M_{\odot}/h$)	c_{vir} ^b	M_{200} ($10^{14} M_{\odot}/h$)	c_{200} ^b	$\chi^2_{\text{min}}/\text{d.o.f}$
NFW	$\gamma = 1$	$7.19^{+0.53}_{-0.50}$	$5.41^{+0.49}_{-0.45}$	$5.98^{+0.40}_{-0.38}$	$4.22^{+0.40}_{-0.36}$	7.2/12
gNFW	$\gamma = 1.27^{+0.24}_{-0.37}$	$7.50^{+0.74}_{-0.65}$	$4.88^{+0.86}_{-0.86}$	$6.15^{+0.48}_{-0.44}$	$3.79^{+0.69}_{-0.69}$	6.6/11
Einasto	$\alpha = 0.188^{+0.062}_{-0.058}$	$7.49^{+0.86}_{-0.73}$	$4.92^{+0.57}_{-0.80}$	$6.15^{+0.50}_{-0.45}$	$3.82^{+0.48}_{-0.66}$	6.6/11

^a Parameter describing the shape of the mass density profile on small scales.

^b NFW-like concentration parameter defined by $c_{\Delta}^{\text{NFW}} = r_{\Delta}/r_s$, $c_{-2}^{\text{gNFW}} = (r_{\Delta}/r_s)/(2 - \gamma)$ and $c_{\Delta}^{\text{Einasto}} = r_{\Delta}/r_{-2}$.

parable with the differences between the predictions from different numerical simulations (Fig. 4). Indeed the observed concentration parameter exceeds the predicted concentration of simulated clusters (Duffy et al. 2008; Zhao et al. 2009; Bhattacharya et al. 2011; De Boni et al. 2012). Prada et al. (2012) recently noted that their mass-concentration relation from four simulations each comprising 10^7 particles agrees better

with observations than previous work. Our best-fit concentration is slightly lower than that of Prada et al..

The NFW model fit ($\chi^2_{\text{min}}/\text{d.o.f.} = 7.2/12$) does not motivate fitting more flexible models to our data (Table 1). For completeness, we fit the generalized NFW (gNFW) and Einasto (1965) profiles. The former adds a free parameter γ to the NFW profile: $\rho \propto x^{-\gamma}(1+x)^{-3+\gamma}$; the latter describes the shape of the profile slope:

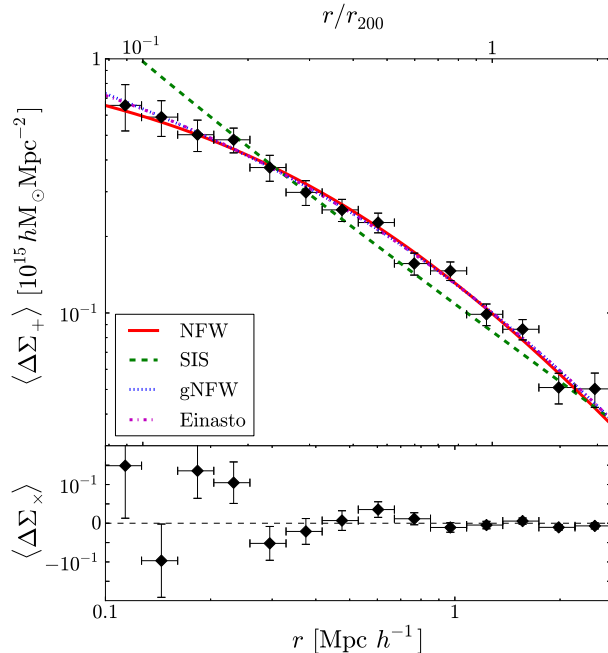


FIG. 3.— Stacked tangential shear profile of all 50 clusters in units of projected mass density, where different cluster and background galaxy redshifts galaxies are weighted by the lensing kernel (Mandelbaum et al. 2006; Okabe et al. 2010; Oguri & Takada 2011; Umetsu et al. 2011). The projected radius is computed from the weighted mean cluster redshift ($z_{\text{cluster}} \simeq 0.23$). The solid, dashed, dotted and dashed-dotted curves are the best-fit Navarro-Frenk-White (NFW), singular isothermal (SIS), generalized NFW (gNFW) and Einasto profiles, respectively. The lower panel shows the result of the 45° test for systematic errors.

$d \log \rho / d \log r = -2(r/r_{-2})^\alpha$, where r_{-2} is the radius at which the slope is isothermal.

The best-fit gNFW profile is consistent with NFW, with $\gamma = 1.27^{+0.24}_{-0.37}$. The best-fit Einasto profile has $\alpha = 0.19 \pm 0.06$, consistent with numerical simulations, e.g. $\langle \alpha \rangle = 0.175 \pm 0.046$ (Gao et al. 2012), and $\langle \alpha \rangle = 0.183$ (Navarro et al. 2004). We also measure the inner slope of the best fit density profile models directly, obtaining $\beta(r = 0.01r_{200}) = -d \log \rho / d \log r = 1.1$ for the gNFW and Einasto models, in good agreement with $\langle \beta \rangle \simeq 1.1$ (Navarro et al. 2004; Gao et al. 2012). This underlines that a constant power law slope is strongly disfavored; we obtain $\chi^2_{\text{min}}/\text{d.o.f.} = 44/13$ for the singular isothermal sphere (SIS) model ($\beta = 2$).

We examine the possible impact of adiabatic contraction on the total measured density profile (Gnedin et al. 2004) by introducing a central point mass contribution as an additional free parameter. We obtain an upper limit on the point mass of $M_{\text{point}} \lesssim 12 \times 10^{12} h^{-1} M_\odot$, which is degenerate with the structural parameters of the smooth component in all models (NFW, gNFW, and Einasto). The best-fit mass and concentration parameters do not change significantly from those listed in Table 1. The excellent fit of the NFW model – that is based on numerical dark matter only simulations – to our weak-lensing data, and the results of adding baryons to the model (albeit in a simplified form) suggest the dark matter may not suffer adiabatic contraction by baryons in the cluster core. We will return to this topic in future more detailed study,

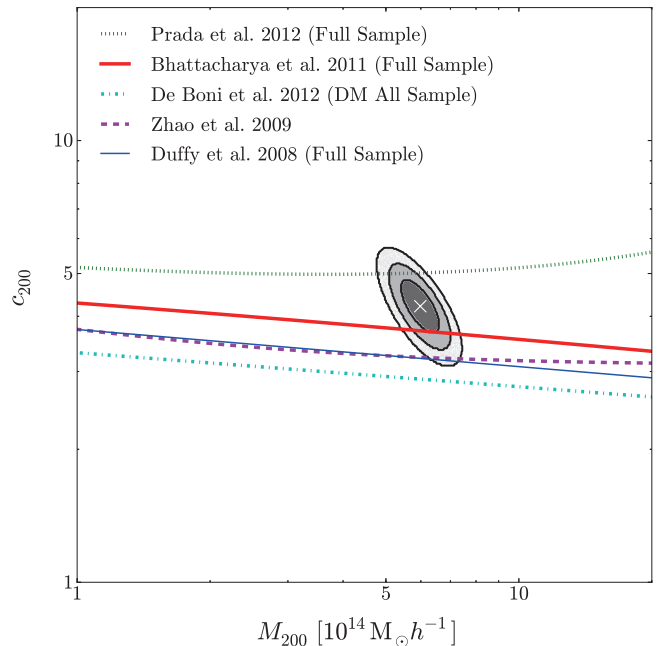


FIG. 4.— Stacked weak-lensing constraints on the mass and concentration of a complete volume-limited sample of 50 galaxy clusters at $\langle z \rangle = 0.23$. The white cross denotes the best-fit parameters and the contours show the 68.3%, 95.4%, and 99.7% confidence levels. Note that the predicted relations have all been converted to be consistent with our analysis.

combining both strong- and weak-lensing constraints.

We also checked whether the results are affected by adopting the BCG as the center of each cluster, by adding an off-centering parameter $\sigma_{R_{\text{off}}}$ to the models following Johnston et al. (2007). The best-fit M_{vir} and c_{vir} are unchanged, and we obtain an upper limit of $\sigma_{R_{\text{off}}} < 29 h^{-1} \text{kpc}$.

4. SUMMARY

We have used sensitive high resolution observations with Subaru to measure the average density profile of a statistically complete volume-limited sample of 50 X-ray luminous galaxy clusters at $0.15 < z < 0.3$. Careful treatment of systematic errors indicate that they are all smaller than the statistical errors. In particular, we achieve just 1% contamination of the background galaxy sample by foreground and cluster galaxies, tests on simulated data indicate that our shape measurement multiplicative systematic error is $m \lesssim 0.03$, and errors from choice of binning scheme are just a few per cent. When the signal from all 50 clusters is combined together we achieve a number density of background galaxies of $266.3 \text{ arcmin}^{-2}$; $\sim 200,000$ galaxies in total.

The shape of the stacked density profile is consistent with numerical simulations across the radial range $100 h^{-1} \text{kpc} - 2.8 h^{-1} \text{Mpc}$. Specifically, we find no statistical evidence for departures from the NFW profile. We constrain the mean mass and concentration of the clusters to sub-10% precision, obtaining $c_{\text{vir}} = 5.41^{+0.49}_{-0.45}$. This level of precision is comparable with the differences between the concentrations predicted by different numerical simulations, and therefore opens the possibility of discriminating between different simulations using observational data in the near future.

Our results emphasise the power of stacked weak-

lensing for constraining to high precision the average mass and shape of galaxy clusters. Imminent surveys such as Hyper Suprime-Cam on Subaru, the Dark Energy Survey, and KIDS, all hold much promise for similar studies of less massive clusters, and clusters at higher redshifts. However significant advances on the precision that we have achieved here on massive low redshift clusters await future facilities such as LSST and *Euclid*. This is because only they will probe sufficiently deep and wide to improve on the number density of background galaxies on our sample of rare massive low redshift clusters, that is drawn from the *ROSAT* All Sky Survey.

ACKNOWLEDGMENTS

We thank Ian McCarthy, Yannick Bahé, and Joop Schaye for sharing their weak shear catalogs from the Cosmo-OWLS simulation in advance of publication. We also thank our LoCuSS colleagues, especially Dan Mar-

rone, Gus Evrard, Pasquale Mazzotta, Arif Babul, and Alexis Finoguenov for many helpful discussions and comments. We acknowledge the Subaru Support Astronomers, plus Paul May, Chris Haines, and Mathilde Jauzac, for assistance with the Subaru observations. We are grateful to N. Kaiser and M. Oguri for making their IMCAT and GLAFIC packages public. This work is supported in part by Grant-in-Aid for Scientific Research on Priority Area No. 467 “Probing the Dark Energy through an Extremely Wide & Deep Survey with Subaru Telescope”, by World Premier International Research Center Initiative (WPI Initiative), MEXT, Japan, and by the FIRST program “Subaru Measurements of Images and Redshifts (SuMIRe)”. GPS acknowledges support from the Royal Society. KU acknowledges partial support from the National Science Council of Taiwan (grant NSC100-2112-M-001-008-MY3) and from the Academia Sinica Career Development Award.

REFERENCES

- Bahé, Y. M. and McCarthy, I. G. & King, L. J., 2012, *MNRAS*, 421, 1073.
- Bhattacharya, S., Habib, S., Heitmann, K., & Vikhlinin, A. 2011, ArXiv e-prints
- Böhringer, H., Schuecker, P., Guzzo, L., et al. 2004, *A&A*, 425, 367
- Broadhurst, T., Umetsu, K., Medezinski, E., Oguri, M., & Rephaeli, Y. 2008, *ApJ*, 685, L9
- Bullock, J. S., Kolatt, T. S., Sigad, Y., et al. 2001, *MNRAS*, 321, 559
- De Boni, C., Ettori, S., Dolag, K., & Moscardini, L. 2012, ArXiv e-prints
- Dolag, K., Bartelmann, M., Perrotta, F., et al. 2004, *A&A*, 416, 853
- Duffy, A. R., Schaye, J., Kay, S. T., & Dalla Vecchia, C. 2008, *MNRAS*, 390, L64
- Ebeling, H., Edge, A. C., Allen, S. W., et al. 2000, *MNRAS*, 318, 333
- Ebeling, H., Edge, A. C., Böhringer, H., et al. 1998, *MNRAS*, 301, 881
- Eisenstein, D. J., Weinberg, D. H., Agol, E., et al. 2011, *AJ*, 142, 72
- Gao, L., Navarro, J. F., Frenk, C. S., et al. 2012, *MNRAS*, 425, 2169
- Gavazzi, R., Fort, B., Mellier, Y., Pelló, R., & Dantel-Fort, M. 2003, *A&A*, 403, 11
- Gnedin, O. Y., Kravtsov, A. V., Klypin, A. A., & Nagai, D. 2004, *ApJ*, 616, 16
- Hennawi, J. F., Dalal, N., Bode, P., & Ostriker, J. P. 2007, *ApJ*, 654, 714
- Heymans, C., Van Waerbeke, L., Bacon, D., et al. 2006, *MNRAS*, 368, 1323
- Hoekstra, H. 2003, *MNRAS*, 339, 1155
- Hoekstra, H., Hartlap, J., Hilbert, S., & van Uitert, E. 2011, *MNRAS*, 412, 2095
- Ilbert, O., Capak, P., Salvato, M., et al. 2009, *ApJ*, 690, 1236
- Johnston, D. E., Sheldon, E. S., Wechsler, R. H., et al. 2007, ArXiv e-prints
- Kaiser, N., & Squires, G. 1993, *ApJ*, 404, 441
- Kaiser, N., Squires, G., & Broadhurst, T. 1995, *ApJ*, 449, 460
- Kneib, J.-P., Hudelot, P., Ellis, R. S., et al. 2003, *ApJ*, 598, 804
- Komatsu, E., Smith, K. M., Dunkley, J., et al. 2011, *ApJS*, 192, 18
- Ludlow, A. D., Navarro, J. F., White, S. D. M., et al. 2011, *MNRAS*, 415, 3895
- Mandelbaum, R., Seljak, U., Cool, R. J., et al. 2006, *MNRAS*, 372, 758
- Massey, R., Heymans, C., Bergé, J., et al. 2007, *MNRAS*, 376, 13
- McCarthy, I. G., Schaye, J., Bower, R. G., et al. 2011, *MNRAS*, 412, 1965
- Miyazaki, S., Komiyama, Y., Sekiguchi, M., et al. 2002, *PASJ*, 54, 833
- Navarro, J. F., Frenk, C. S., & White, S. D. M. 1997, *ApJ*, 490, 493
- Navarro, J. F., Hayashi, E., Power, C., et al. 2004, *MNRAS*, 349, 1039
- Neto, A. F., Gao, L., Bett, P., et al. 2007, *MNRAS*, 381, 1450
- Oguri, M. 2010, *PASJ*, 62, 1017
- Oguri, M., Bayliss, M. B., Dahle, H., et al. 2012, *MNRAS*, 420, 3213
- Oguri, M., & Takada, M. 2011, *Phys. Rev. D*, 83, 023008
- Oguri, M., Hennawi, J. F., Gladders, M. D., et al. 2009, *ApJ*, 699, 1038
- Okabe, N., Takada, M., Umetsu, K., Futamase, T., & Smith, G. P. 2010, *PASJ*, 62, 811
- Okura, Y., & Futamase, T. 2012, *ApJ*, 748, 112
- Popesso, P., Biviano, A., Böhringer, H., Romaniello, M., & Voges, W. 2005, *A&A*, 433, 431
- Prada, F., Klypin, A. A., Cuesta, A. J., Betancort-Rijo, J. E., & Primack, J. 2012, *MNRAS*, 423, 3018
- Schlafly, E. F., & Finkbeiner, D. P. 2011, *ApJ*, 737, 103
- Smith, R. E., Peacock, J. A., Jenkins, A., et al. 2003, *MNRAS*, 341, 1311
- Springel, V., Wang, J., Vogelsberger, M., et al. 2008, *MNRAS*, 391, 1685
- Umetsu, K., Broadhurst, T., Zitrin, A., et al. 2011, *ApJ*, 738, 41
- Umetsu, K., Medezinski, E., Broadhurst, T., et al. 2010, *ApJ*, 714, 1470
- Wu, H.-Y., Hahn, O., Wechsler, R. H., Mao, Y.-Y., & Behroozi, P. S. 2012, ArXiv e-prints
- Zhao, D. H., Jing, Y. P., Mo, H. J., & Börner, G. 2009, *ApJ*, 707, 354